Chapter 5

Vacuum annealed AZO films deposited by spray pyrolysis

5.1 Introduction

Spray pyrolysis is a solution-based thin film processing technique that is suitable for mass production and is inexpensive in comparison to vapor-based processing routes. The temperature of the hot plate/substrate, pressure and spray medium, and height of the spray nozzle are some of the important parameters which decide the microstructure and quality of the deposited films [253]. In comparison to solution-based techniques, films processed by vapor-based techniques exhibit good transparency and conductivity which is attributed mainly to the superior grain orientation, crystal quality, and, carrier concentration [170,234,254,255]. Solution-processed films can also be thermally annealed in a vacuum and reducing atmospheres to improve the electrical and optical properties mainly through the introduction of defects such as oxygen vacancies (V_O) [256], Zn interstitial (Zn_i) [201], anti-site defects [257], hydrogen incorporation [258] and improving surface morphology [259]. Earlier studies suggest the generation of oxygen vacancies (V_O) leaves electrons close to the conduction back; however, in recent years, it has been shown that the ionization energy of Zn interstitials (Zn_i) are much lower than that of V_O and are responsible for the increase in carrier concentration thereby conductivity.

To develop a high throughput solution-based processing for ZnO-based TCOs, it is important to device ways to improve the performance of solution-processed films at par with the vacuum processing techniques. Therefore, insight into the defects and crystal quality as a function of processing is a prerequisite. Although there are many in-depth studies on the defects and crystal orientation and their effect on the electronic properties of films processed by vacuum-based techniques[260,261]; however, reports of similar in-depth studies for solution-based processed films are scarce.

In this chapter, we have discussed AZO thin film deposition by spray pyrolysis to obtain highly transparent and conductive thin films. As-deposited films were vacuum annealed (7.8 torrs) for 20 min. Structural, morphological, optical, surface-specific electrical properties of pure ZnO and 1 at.% Al-doped ZnO(1AZO) was investigated. The effect of doping and defects introduced as a result of vacuum annealing on the electronic band energies is discussed in detail. After vacuum annealing, a resistivity as low as ~$2x10^{-3}$ Ω-cm, transparency ~82% at 550 nm, and a figure of merit as high as 1.44 was achieved, which is closer to the vapor-based processing technique. In the description of this chapter 1 at%, Al-doped ZnO (1AZO), or 1 at% Al has a similar meaning.

5.2 Result and discussion

5.2.1 X-ray diffraction

X-ray diffraction (XRD) patterns of the pure and 1 at% Al-doped ZnO (1AZO) thin films are shown in **Figure 5.1**. The XRD pattern of the as-deposited ZnO and 1AZO films could be indexed to the wurtzite structure. In the case of as-deposited ZnO

films, the most intense XRD peak was from the (100) plane. On the other hand, in the case of 1AZO films, only the (002) peak was intense while the other peaks were barely visible. This indicates that the pure ZnO had a tendency to partially orient along (100) direction, while the 1AZO films were oriented along [002] direction. On vacuum annealing, the ZnO films became almost perfectly oriented along (002), while the orientation of the 1AZO films remained unchanged[262]. The quantitative information concerning the preferential orientation was obtained from the texture coefficient [263,264]. The texture coefficient of the (002) plane is determined from the XRD pattern using equation 5.1.

$$T_c(hkl) = \frac{I_{hkl}/I_{0\ hkl}}{\frac{1}{N}\sum_1^N \frac{I_{hkl}}{I_{o\ hkl}}} \qquad 5.1$$

where $T_c(hkl)$ is the texture coefficient of the *(hkl)* plane, I_{hkl} is the relative intensity of the *(hkl)* plane, and $I_{o(hkl)}$ is the relative intensity of the XRD reference of the randomly oriented grains in the *(hkl)* plane, N is the number of diffraction peaks considered. The variation of $T_c(hkl)$ for the (002) plane of all the films is listed in **Table 5.1**. For a randomly oriented film, the $T_c(002)$ should be close to one, while $T_c(002)$ greater than one indicates texturing along (002) direction. The as-deposited pure ZnO had a $T_c(002)$ close to 0.91 indicating the absence of any texture, while on vacuum annealing, $T_c(002)$ of the films increased to 5.53. On the other hand, the synthesized 1AZO films had a $T_c(002)$ close to 11.6, which reduced slightly to 8.2 on vacuum annealing [265]. This indicates that both vacuum annealing and aluminum doping favored the texturing of the films. The slight reduction in the texture parameter on vacuum annealing of 1AZO films could be attributed to the

reduced crystallinity due to the generation of defects either by the creation of oxygen vacancies (V_O) or the release of stress. Since, V_O generation would ideally happen on both the undoped and doped samples, the generation/alignment of defects such as dislocation during stress relaxation might have been the reason for this observed reduction in the peak intensity on vacuum annealing, as has also been reported earlier [96,266,267]. The crystallite sizes along (002) were calculated using the Scherrer formula (listed in **Table 5.1**). On vacuum annealing, pure ZnO films became preferentially oriented in (002) direction while the crystallite size became larger[96].

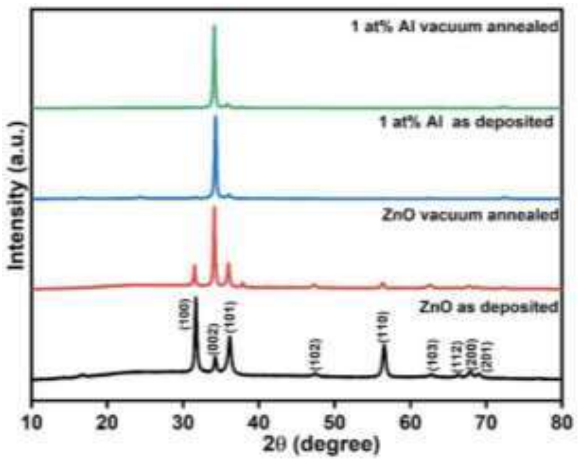

Figure 5.1 X-ray diffraction pattern of undoped and 1AZO as-deposited and vacuum-annealed film

Table 5.1 Lattice parameters (a and c), crystallite size, and texture co-efficient (T_C) of the pure ZnO film, 1AZO films, and ZnO bulk reference. ZnO bulk reference data adapted from the database (JCPDS number:00-003-0888)

Sample	*a* (nm)	*c* (nm)	V (nm^3)	Crystalline size (nm)	Texture coefficient
Bulk*ZnO	0.325	0.521	0.047	-	-
As deposited					
Pure ZnO	0.326	0.523	0.048	21	0.91
1AZO	0.327	0.524	0.048	29	11.6
After vacuum annealing					
Pure ZnO	0.328	0.526	0.049	32	5.53
1AZO	0.328	0.525	0.049	31	8.2

5.2.2 Scanning electron microscopy

Scanning electron microscopy (SEM) was carried out to analyze the morphology and coverage. It can be observed from secondary electron images (shown in **Figure 5.2a**) that the grains of as-deposited pure ZnO films were composed of smaller crystallites with an elongated morphology. On the other hand, the 1AZO films mainly had uniform spherical grains with a dimension of ~0.3μm (**Figure 5.2b**). Cross-sectional SEM images showed random grains in pure ZnO films (**Figure 5.2c**), while in the case of doped films, the grains were elongated along the thickness (**Figure 5.2d**). This indicates that in the case of pure ZnO films, the grains must have grown along the [100] direction giving rise to the higher intensity of (100) peaks in XRD while, in 1AZO film, the rod-like morphology protruding out of the substrate surface along [002] direction resulted in near perfect orientation in the doped films as observed from the XRD. After vacuum annealing, pure ZnO films had random elongated grains (approx. ~0.8 μm in length, shown in **Figure**

5.2e), while the doped films had elongated grains (**Figure 5.2f**). In all the cases, the grains were composed of nanocrystals, as observed from the X-ray broadening of peaks. Similar morphological features were reported earlier for the spray-deposited pure and Al-doped ZnO films [203,268]. It was clear from observed X-ray diffraction patterns that preferential growth took place during the spray pyrolysis of the 1AZO films, which remain intact on vacuum annealing, while at the same time, became more compact as observed from the SEM micrograph in **Figure 5.2f**. On the other hand, the as-deposited pure ZnO films were composed of elongated morphology with nanocrystalline grains, which on vacuum annealing became oriented along [002] direction similar to the doped film and also became compact.

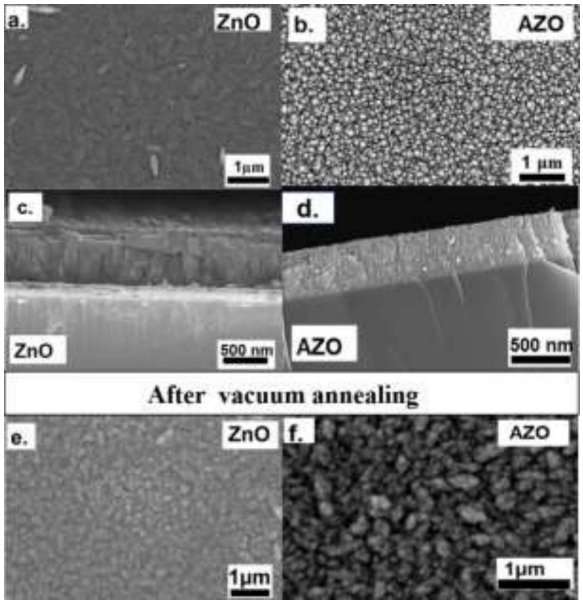

Figure 5.2 HR SEM images of a) Pure ZnO film, b) 1AZO films, c) cross-sectional view of pure ZnO films, d) cross-sectional view of 1AZO films, e) ZnO film after vacuum annealing, and f) 1AZO film after vacuum annealing

5.2.3 Atomic force microscopy

Surface morphology plays a significant role in determining optical and electrical properties. To identify the effect of doping and vacuum annealing on the surface topography, atomic force microscopy (AFM) was carried out in tapping mode (shown in **Figure 5.3**). For a better insight into the surface topography, AFM images were taken at four random places. Film topography changed significantly on doping with Al. The roughness of the as-deposited ZnO and 1AZO films were ~26.81 nm and ~24.84 nm, respectively (**Figure 5.3a&b**), which on vacuum annealing, decreased to ~18.85 nm and ~14.05 nm for ZnO and 1AZO film, respectively (**Figure 5.3c&d**). The roughness of the film decreases after vacuum annealing due to uniform grain growth. The shape parameter skewness (R_{sk}) and the kurtosis (R_{ku}), which measure the asymmetry and the sharpness of the roughness profiles shown in **Figure 5.4**, respectively, are listed in **Table 5.2**. A positive value of the R_{sk} parameter indicates that the height distribution is asymmetrical with more peaks than valleys. The enhanced surface diffusion during annealing results in increased R_{sk}, R_{ku} was < 3 for pure ZnO in both the cases of as-deposited and vacuum annealed films, which signified that the film had fewer peaks than valleys, while for the 1AZO films, R_{ku} was slightly less than 3 in as-deposited condition, which increased to 3.23 on vacuum annealing[261,269]. The topography of the Al-doped ZnO films was like aligned rods. The waviness of the films decreased from ~60 nm for pure ZnO films to ~6 nm for 1AZO.

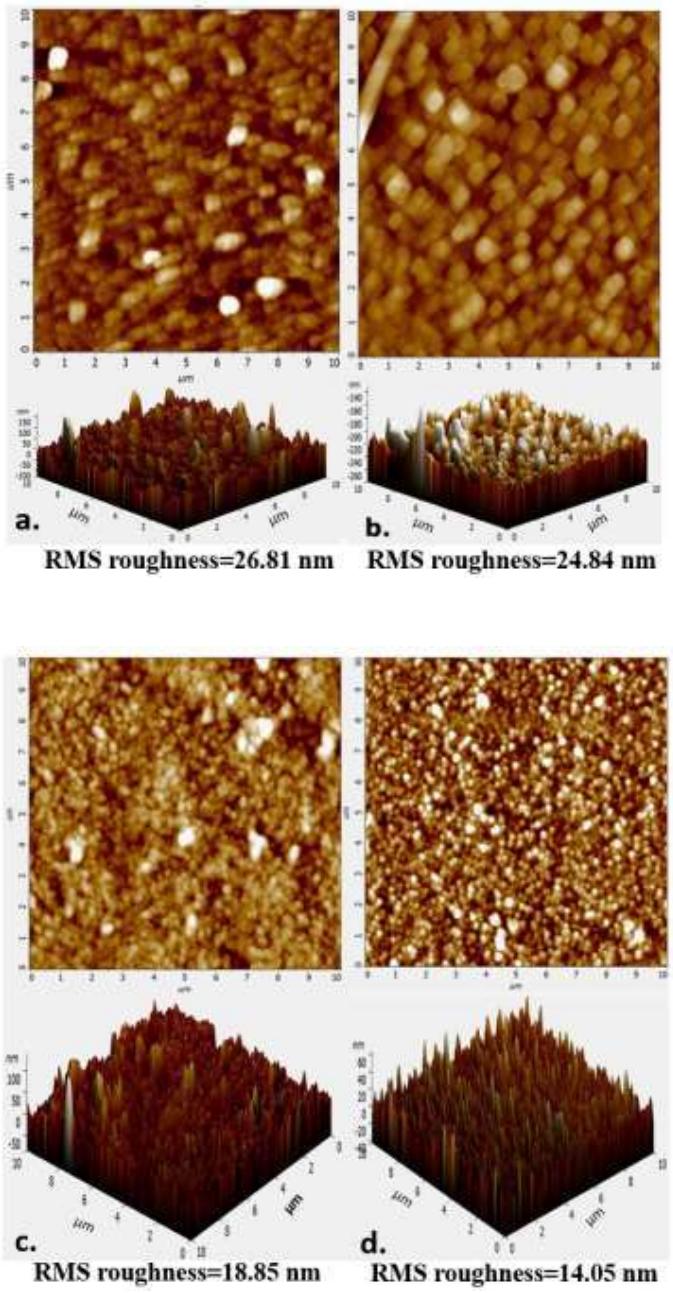

Figure 5.3 Surface topography images of as-deposited(a) ZnO, (b) 1AZO film and vacuum annealed, (c) ZnO, and (d) 1AZO film

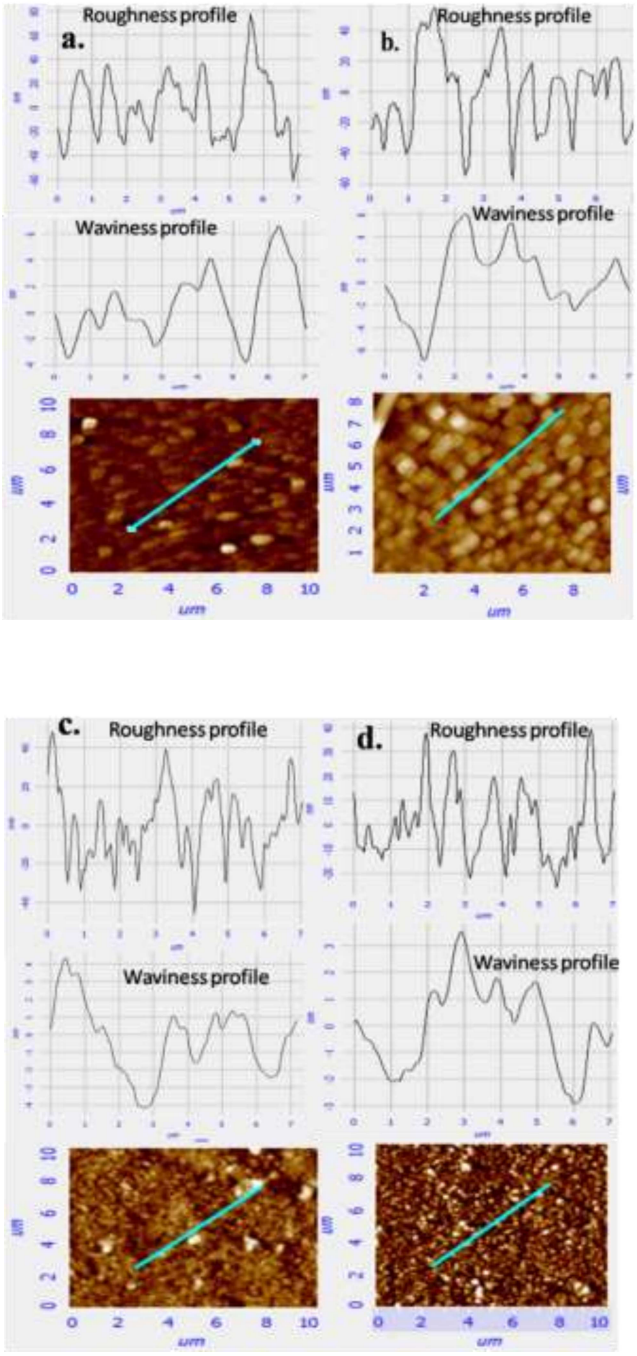

Figure 5.4 Roughness and waviness profile of a) as deposited ZnO b) as deposited 1AZO c) vacuum annealed ZnO d) vacuum annealed 1AZO thin film

Table 5.2 Roughness parameters of as-deposited and vacuum-annealed ZnO and 1AZO thin films

Sample	R_a (Arithmetical mean deviation of profile)	R_q(Root-mean-square deviation of profile)	R_{sk} (Skewness of profile)	R_{ku} (Kurtosis of profile)
		As deposited		
ZnO	22.16 nm	26.45 nm	0.33	2.72
1AZO	20.62 nm	25.15 nm	0.00071	2.41
		Vacuum annealed		
ZnO	15.19 nm	18.63 nm	0.0026	2.34
1AZO	11.14 nm	14.05 nm	0.72	3.23

5.2.4 Optical properties

To determine the optical properties and bandgap of the pure and doped ZnO thin film UV–visible and photoluminescence spectroscopy was carried out. Both doped and undoped ZnO films were >80% transparent in the visible and IR regions, as can be observed from **Figures 5.5a&b**. The optical bandgap energy (E_g) was calculated using the Tauc plot. The bandgap of films increased on doping and vacuum annealing. For instance, the bandgap of pure ZnO films increased from 3.21 ± 0.02 to 3.27 ± 0.02 eV, while for AZO films, the bandgap increased from 3.31 ± 0.02 to 3.4 ± 0.02 eV on vacuum annealing (shown in **Figure 5.5c&d**)[94,204]. The increase in the optical bandgap could be explained by the Burstein Moss (BM) effect [270,271]. The extra electron from the dopant Al substitution and point defects, particularly V_O, and Zn_i, generated due to vacuum annealing, occupies the lower energy conduction band states. The BM effect shifts the optical absorption edge giving a higher effective bandgap due to the larger energy gap between

occupied states at the top of the valence band and unoccupied states in the conduction band[39,184].

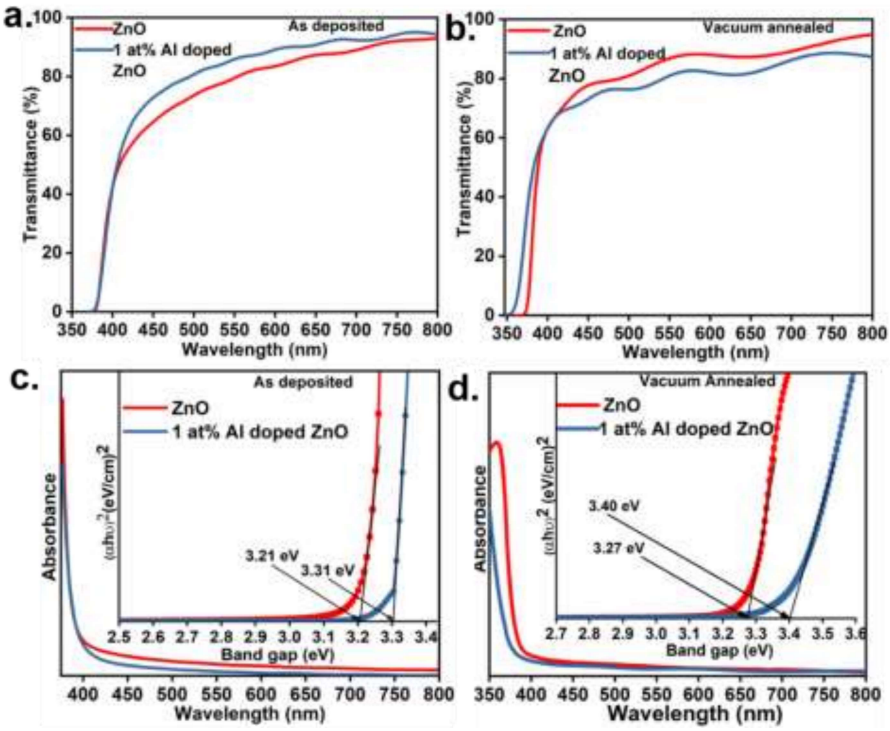

Figure 5.5 a) & c) Transmittance as a function of wavelength of ZnO and 1AZO of as-deposited and vacuum annealed thin film respectively, b) & d) absorbance plot of ZnO and 1AZO thin film (inset shows the Tauc plot) of as-deposited and vacuum annealed, respectively

Photoluminescence spectra of as-deposited and vacuum annealed ZnO and 1AZO films were recorded at an excitation wavelength of 325 nm (shown in **Figure 5.6**). Two broad luminescence peaks with shoulders were observed in the wavelength range of 340 nm to 650 nm. The photoluminescence peaks could be deconvoluted to four main peaks with slightly shifted positions (corresponding to energies in the

range 3.20-3.36 (a), ~3.1 (b), ~2.9 (c) and ~2.44 (d) eV), which were attributed to the radiative recombination at band edge, Al at Zn sites (Al_{Zn}) or Zn_i (+2/+1), ex-Zn_i (+1/0), and V_o respectively [272,273]. One such fitted spectrum of 1AZO film is shown in **Figure 5.7a**. The presence of shallow donors such as Zn_i and Al_{Zn} is known to decrease the resistivity of ZnO films. The intensity of the defect peaks b, c, and d was normalized against the band edge PL intensity (shown in **Figure 5.7b**). The peaks corresponding to the Zn_i and V_O both increased significantly on vacuum annealing as shown in **Figure 5.7b**. A clear band edge peak is visible in the PL spectrum of ZnO film (**Figure 5.6**), which is partially masked in other samples due to an increase in the intensity of peak b on vacuum annealing or doping. This observation was in-line with the observation that annealing in an oxygen-deficient atmosphere results in the creation of V_O and Zn_i [272,274,275].

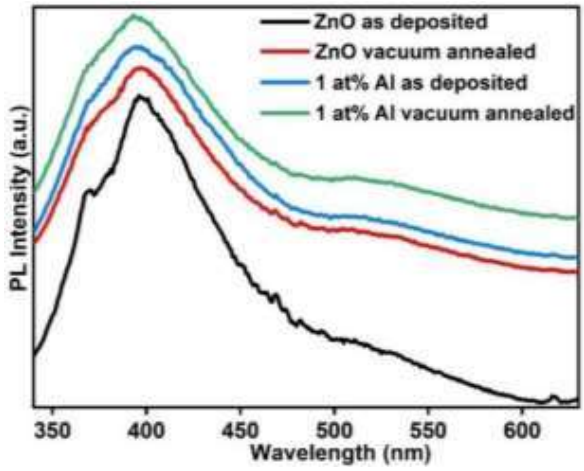

Figure 5.6 Photoluminescence of zinc oxide and 1AZO thin film as deposited and vacuum annealed

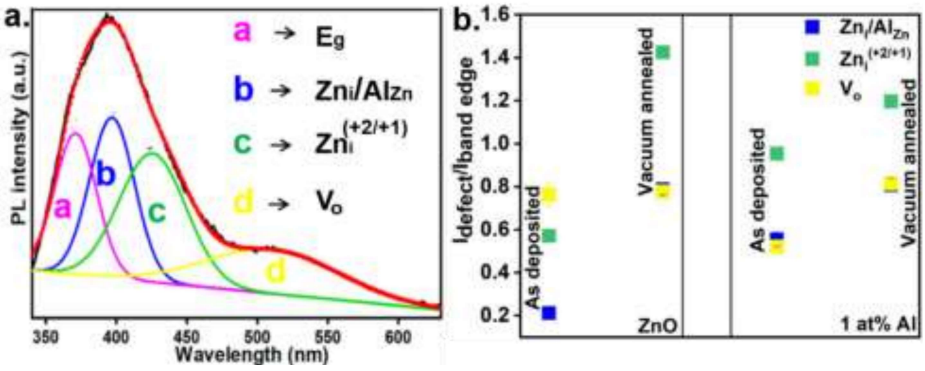

Figure 5.7 a) A fitted PL spectrum of 1AZO films, and b) Normalized intensity of PL peaks from defect level

5.2.5 X-ray photoelectron spectroscopy (XPS)

X-ray photoelectron spectroscopy (XPS) was carried out to get the surface-specific compositional analysis and oxidation state of Zn, O, and Al. The binding energy scale was charge-referenced using the adventitious carbon C1s peak positioned at 284.8 eV[276]. XPS of O1s was used to inspect the chemical state of oxygen in pure ZnO and 1AZO films (**Figure 5.8**). In the case of pure ZnO, the O1s binding energy peak was centered at ~529.9 eV[33,267], while for 1AZO, the O1s peak was at 530.47 eV. On vacuum annealing, the O1s peaks shifted towards higher binding energies 530.98 and 530.93 eV for ZnO and 1AZO films, respectively (shown in **Figure 5.8**) [33,267,277]. The shift towards higher binding energy could be due to the decrease in adsorbed oxygen (O_{Ads}). On Al doping, the peak shifting to a slightly higher binding energy was attributed to the greater affinity of Al for oxygen. All the observed shifts in the binding energy were in the range of associated defects and characteristic bonds [236,278]. On vacuum annealing, the formation of V_O could be the major reason for the shift in the O1s peak. The O1s peak shape, in all the

cases, was asymmetric with a tail-like feature toward the higher binding energy. The wide scan of the O1s peak could be deconvoluted into three peaks, as shown in **Figure 5.9**. The peak at the lower binding energy close to 530.3±0.3 eV (Peak I) was attributed to fully coordinated oxygen in the lattice (O_{Lat}). This could be the Zn-O bond in the case of the pure ZnO sample, while in the case of 1AZO, this could be oxygen bonded to Al or Zn. The higher binding energy component of the O1s peak (~531.1±0.03 eV, hereafter called Peak II) was associated with O^{-2} ions that are in the oxygen-deficient region (O_{Vac}). Any change in the intensity of peak II could be partly connected to the variation in the concentration of oxygen defects (V_O or O_i). The third deconvoluted peak component was at binding energy close to 532.4±0.06 eV (Peak III), which could be attributed to the chemically adsorbed oxygen (O_{Ads}) through the atmospheric contaminants such as -CO_3^{-2}, water, and hydroxyl groups. The presence of V_O or O_i (characterized by the peak II at ~531.1±0.03 eV) plays an important role in the conductivity of the ZnO-based thin films [33,177,279,280]. It was observed that in both the cases of ZnO and 1AZO films, the area under peak II increased on vacuum annealing, which indicated the increased concentration of V_O (shown in **Table 5.3**). The concentration ratios O_{Vac}/O_{Lat} and O_{Ads}/O_{Lat} (shown in Table 5.3) were estimated from the corresponding peak intensities. The O_{Ads}/O_{Lat} ratio decreased while the O_{Vac}/O_{Lat} ratio increased on vacuum annealing of ZnO and 1AZO films. The Zn2p transition for all the films shows the typical doublet corresponding to Zn2p1/2 and Zn2p3/2 separated by 23.14 eV with the Zn 2p3/2 peaks appearing around 1022 eV[234](**Figure 5.10**). In the case of pure ZnO films, the Zn 2p3/2 peak was observed at 1021.30±0.1 eV [29], which shifted on vacuum annealing to

1022.20±0.1 eV, as shown in **Figure 5.11**. This indicates gradual modification of the surface configuration of the ZnO matrix from Zn-rich condition to stoichiometric ZnO [213,280]. This result is rather puzzling as, in this case, annealing was carried out in an oxygen-deficient environment, which should ideally shift the Zn 2p3/2 peaks towards lower binding energy. A similar puzzling result was observed earlier in the case of ZnO nanorods, where Zn 2p3/2 was observed to shift towards higher binding energy on annealing in the vacuum, which was attributed to the surface adsorbed oxygen forming Zn-O bonds on annealing[213]. On the other hand, in the case of 1 at% Al-doped ZnO, the Zn2p3/2 peak appeared at 1021.7±0.1 eV[33] in as-deposited film, which shifted to 1021±0.1 eV on vacuum annealing as shown in **Figure 5.11**. This indicates that in as-deposited conditions, the Al-doped ZnO was closer to the stoichiometric ZnO, and on vacuum annealing, the surface became deficient in oxygen resulting in the formation of more Zn-Zn bonding. This could also be attributed to the changes in the terminating surface due to doping. It can be argued that the as-deposited ZnO had Zn^{2+} as terminating ions with O_{Ads} species at the surface, which on annealing, were able to form some Zn-O bonds. While in the case of 1AZO samples, Zn^{2+} ions might not be the dominant terminating ions due to the presence of Al which binds the oxygen much more strongly. The Zn2p3/2 peak shifted in the opposite direction on vacuum annealing for the pure and doped samples. In the case of undoped films, the surface was rich in Zn, while in the case of the doped sample, Al could bind oxygen more strongly, resulting in a lesser amount of adsorbed oxygen on the surface after vacuum annealing (as shown in **Figure 5.9d**) of 1AZO film, thus increasing the number of coordinated Zn.

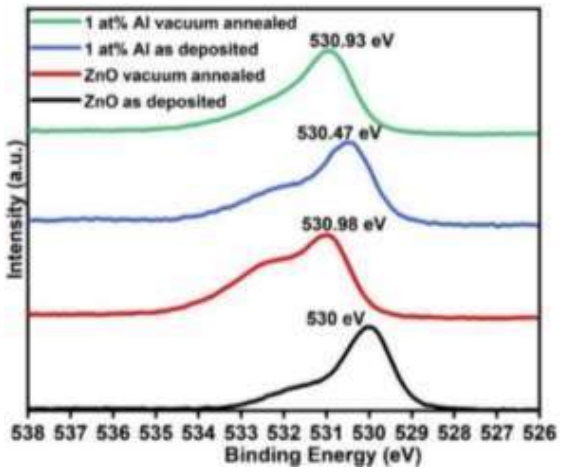

Figure 5.8 XPS of O1s orbital of ZnO and 1AZO films in as-deposited and vacuum-annealed condition

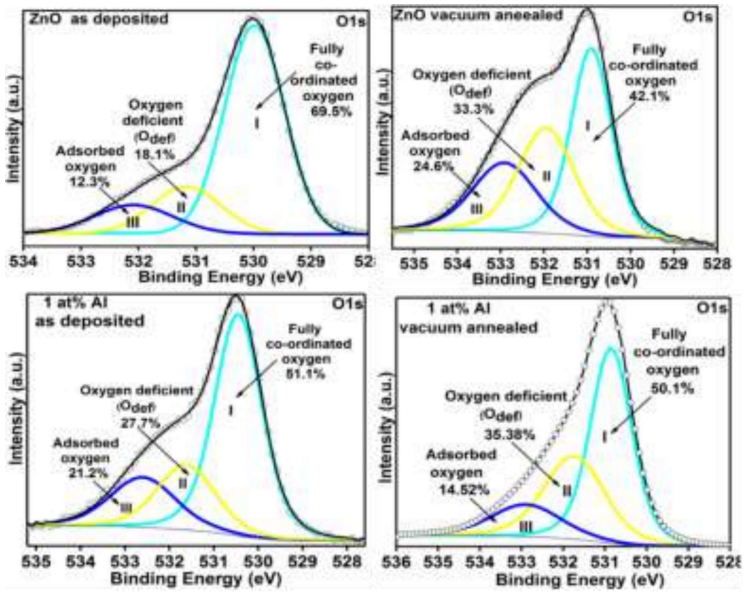

Figure 5.9 XPS of O1s orbital of a) as deposited ZnO, b) ZnO vacuum annealed, c) as deposited 1AZO, and d) vacuum annealed 1AZO

Table 5.3 The trend of V_o/O_{Lat} and O_{Ads}/O_{Lat} in XPS spectra of O1s pure ZnO and 1AZO films as-deposited and vacuum annealed

Sample	V_o/O_{Lat}	O_{Ads}/O_{Lat}
ZnO film as deposited	0.26	0.18
ZnO film after vacuum annealing	0.79	0.58
1AZO film as deposited	0.54	0.41
1AZO film after vacuum annealing	0.70	0.29

A wide scan of the Al2p orbital was carried out for as-deposited and vacuum-annealed 1AZO (shown in **Figure 5.12**). For the 1AZO films, the Al2p peak was observed at 74.0±0.1 eV, which shifted to the higher binding energy of 74.8±0.1 on vacuum annealing. The Al2p peak at 74.0±0.1 eV was attributed to the partial substitution of Al for Zn in the ZnO lattice; however, the shifting of the XPS peak to the higher binding energy could have been due to the formation of Al_2O_3 by oxidation of a fraction of the dopant Al[106,234,280]. This further strengthens our assertion that the adsorbed oxygen can react with alumina on heating and modifying the surface resulting in the opposite shift of Zn2p XPS peak on vacuum annealing of 1AZO. It can be concluded from the XPS analysis that V_O is generated during the vacuum annealing of as-deposited samples, while in the case of the as-deposited films, the Zn-Zn bond was more strongly bonded. This could be attributed to the creation of oxygen vacancies in the vicinity of Zn atoms in the lattice[281]. Therefore, it could be concluded that the concentration of V_O was lower in the case of pure as-synthesized films while Al being more strongly bonded with oxygen, not only favored the creation of oxygen vacancies in the vicinity of Zn but also led to the generation of Zn interstitials[272]. On vacuum annealing, both undoped and Al-

doped samples ended up with a significant increase in the concentration of Zn_i and V_O.

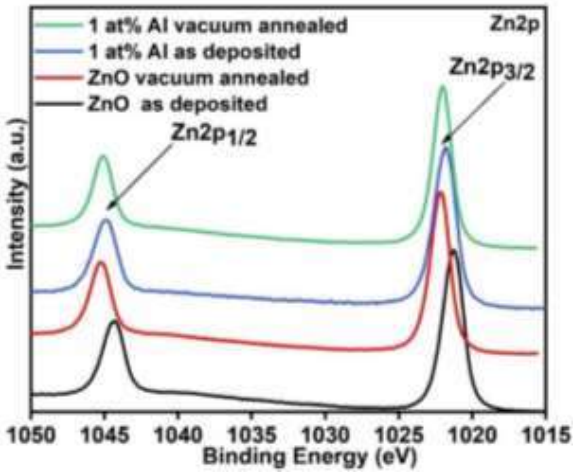

Figure 5.10 XPS of Zn2p orbital undoped and 1AZO thin film in as-deposited and vacuum annealed condition

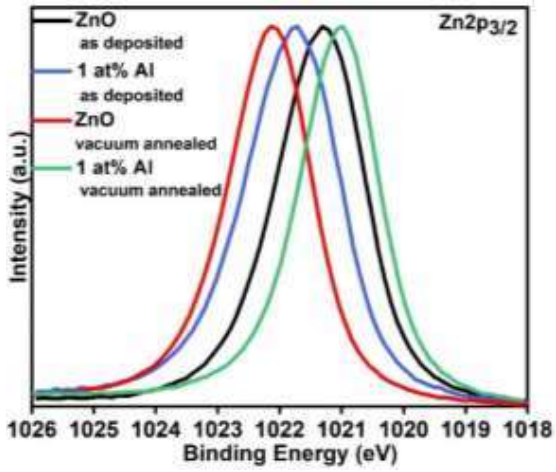

Figure 5.11 Comparative XPS of $Zn2p_{3/2}$ orbital of as-deposited and vacuum-annealed ZnO and 1AZO film

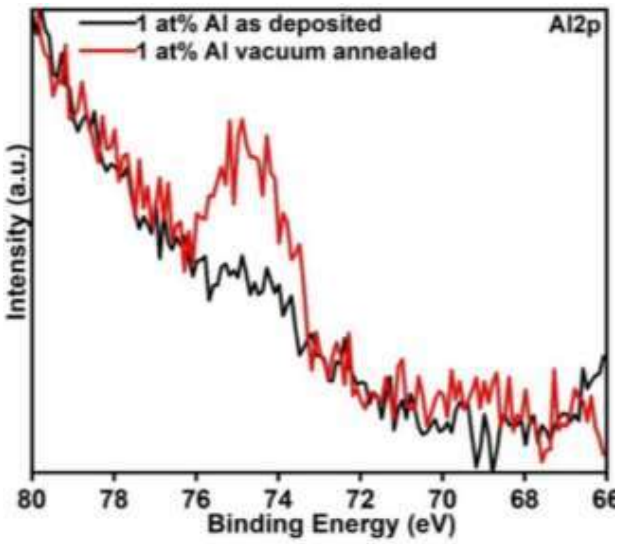

Figure 5.12 X-ray photoelectron spectroscopy of Al2p orbital 1AZO as-deposited and vacuum annealed

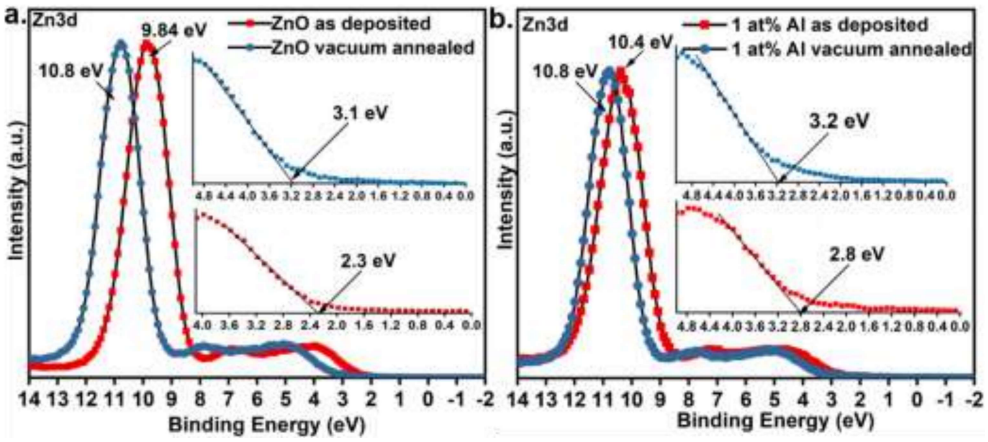

Figure 5.13 Valence band XPS of Zn 3d orbital of zinc oxide thin film a) pure ZnO and b) 1AZO films

The valence band x-ray photoelectron spectra (VB-XPS) of the undoped and Al-doped ZnO in as-deposited and vacuum-annealed conditions are shown in **Figure 5.13**. High-resolution VB-XPS probes the cross-section weighted density of states

in the valence band. All four spectra were aligned with the Fermi level. The peak at a binding energy of 9.84 ± 0.1 eV and 10.4 ± 0.1eV is attributed to Zn3d for as-deposited pure ZnO and 1AZO films, respectively (shown in **Figure 5.13a**), which shifted to 10.81±0.1eV and 10.81±0.1eV, respectively, on vacuum annealing (shown in **Figure 5.13b**). The position of the Fermi level (E_f), determined from the linear extrapolation of the band edge, was 2.3±0.04 eV for the as-deposited ZnO, which on vacuum annealing shifted to 3.14±0.04 eV as shown in **Figure 5.13a**. On the other hand, the Fermi level (E_f) was at 2.8±0.04 eV for 1AZO in an as-deposited state, which shifted to 3.2±0.04 eV on vacuum annealing, as shown in **Figure 5.13b**. On doping, Al in ZnO optical bandgap increased from 3.24 to 3.31 eV, at the same time, a change in Fermi energy level was observed. The shift in the Fermi level was further analyzed by estimating Burstein-Moss (BM) shift energy. Mott-Edwards-Sienko (MES) [39] criterion was adopted to identify the critical metallization density at which the Al^{3+} donor (impurity) states merge with the host (ZnO) CB. MES criterion is represented as equation 5.2

$$n_c^{1/3} a^* \geq 0.26 \qquad 5.2$$

where a^* is the Bohr radius of the isolated donor state, taken as 1.4 nm for n-type donors in ZnO[282]. The critical electron concentration was estimated to be ~6.41x10^{18} cm^{-3}. This employs that the Fermi level would be above CBM for $n>n_c$. The charge carrier concentration obtained from the Hall measurement was ~1.7 x 10^{20} cm^{-3} for vacuum-annealed 1AZO film which was greater than the n_c, indicating that the Fermi level was above the CBM, which was in agreement with the Fermi level obtained from valence band x-ray photoelectron spectroscopy (VBXPS).

VBXPS of the other films also agreed with the obtained result. The BM shift was calculated from equation 5.3

$$\Delta E_{BM} = E_F - E_c = \frac{\hbar^2 (3\pi^2 n)^{2/3}}{2m^*} \qquad 5.3$$

Where $\hbar$ is the Planck constant, m^* is the electron effective mass, and n is the electron density determined from Hall-effect measurements. The effective mass of the electron was assumed as m^*=0.26m_0, and the bottom of the ZnO conduction band is located at the center of the Brillouin zone[39]. Therefore, the effective mass of the electron was assumed to remain constant within the occupied part of the conduction band [283]. The estimated BM shift of pure ZnO and 1AZO are listed in **Table 5.4.**

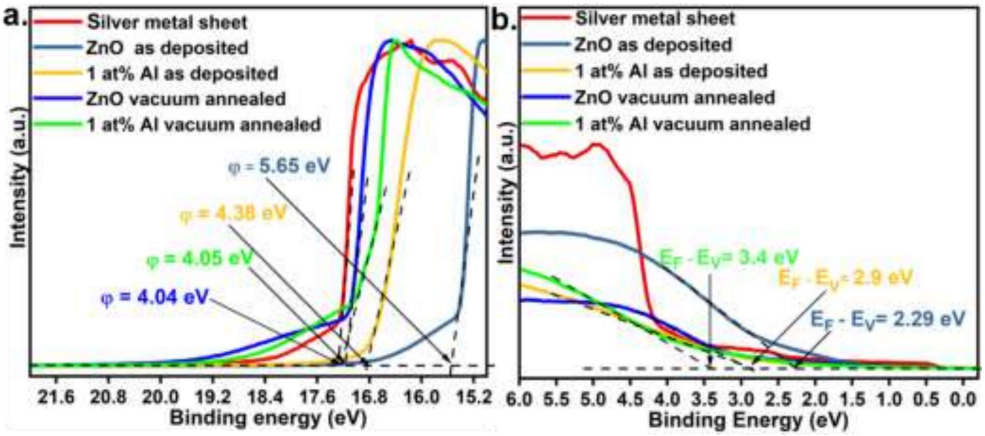

Figure 5.14 (a) High energy cut-off, and (b) valence band onset of UPS spectra recorded for pure ZnO and 1AZO films in as-deposited and vacuum annealed condition

Table 5.4 Electronic and optical properties of ZnO and 1AZO thin films

Sample	Band-gap(E_g) (eV)	BM-shift(eV)	Work function (φ) (eV)	E_F-E_V (eV)
ZnO as deposited	3.21±0.02	0.001	5.65±0.06	2.29±0.02
1AZO as deposited	3.31±0.02	0.02	4.38±0.06	2.8±0.02
ZnO vacuum annealed	3.27±0.02	0.04	4.05±0.06	2.9±0.02
1AZO vacuum annealed	3.4±0.02	0.22	4.04±0.06	3.44±0.02

5.2.6 Ultraviolet photoelectron spectroscopy (UPS)

The electronic work function was estimated from UPS (Ultraviolet photoelectron spectroscopy) by measuring the difference between the Fermi Level and the cut-off energy of the 'tail' at the low kinetic energy end of the spectrum (i.e. spectrum width) and subtracting this value from the incident photon energy which is 21.21 eV for He I ion spectra[284]. UPS allows work-function calculation from a single spectrum. When measuring the electronic work function using UV-photoelectron spectroscopy, it is necessary to apply a small bias (typically 5-10 V) to the sample surface to deconvolute the true work function of the surface from the internal work function of the spectrometer. A bias of -10 eV has been applied during the UPS measurement to overcome this work function[285]. Sputtered silver metal sheet was used as a reference for the measurement of UPS spectra[286]. Considering that the Fermi levels of the analyzer and the investigated sample are equal, one can determine the energy difference between the Fermi level and the valence band onset (E_F-E_V), and work function φ. **Figure 5.14 a&b** shows the high energy cut-off and

valance band onset energy of the UPS spectrum recorded for as-deposited and vacuum-annealed pure ZnO and 1AZO films. The intercept on the binding energy axis line with a linear approximation of high energy cut-off taken between 1/3 and 2/3 of the cut-off's maximum intensity allows the determination of the surface work function [287] (shown in **Figure 5.14a**) of examined samples according to the equation 5.4

$$\varphi = h\nu - E_{cut\text{-}off} \qquad 5.4$$

where $h\nu$ is the excitation energy (21.21 eV), and $E_{cut\text{-}off}$ is the intercept. The obtained work function values are listed in **Table 5.4**. The work function of pure as-deposited ZnO was 5.65 eV which shifted to 4.05 eV on vacuum annealing. On the other hand, the work function of the as-deposited 1AZO film was 4.38 eV, which was reduced to 4.04 eV after vacuum annealing. The values of E_F-E_V were determined to be 2.29 eV for as-deposited zinc oxide and 2.8 eV zinc oxide after vacuum annealing; for 1AZO, it was 2.9 eV for as-deposited film and 3.44 eV after vacuum annealing, respectively, as shown in **Figure 5.14b**. The edge of the valence band maximum was determined by extrapolating the lower binding energy edge to the intersection of the baseline (**Figure 5.14a**) [287–289]. The obtained work function was maximum (5.65±0.02 eV) for the pure as-deposited ZnO films, while the minimum (4.04±0.02 eV) for vacuum annealed 1AZO films. A sharp decrease in work function after vacuum annealing, from 5.65±0.06 eV to 4.05±0.06 eV in the case of ZnO, and from 4.38±0.06 to 4.04±0.06 eV for 1AZO films was observed. Fermi edge shifted towards the conduction band for both ZnO and 1AZO film as is evident from the schematic shown in **Figure 5.15**, due to the increase in

bulk concentration. In ZnO films, the bulk carrier concentration increased from ~10^{16} cm^{-3} to ~10^{18} cm^{-3} on vacuum annealing while in the case of 1AZO films, carrier concentration increased from ~10^{18} cm^{-3} in as-deposited condition to ~10^{20} cm^{-3} after vacuum annealing (listed in **Table 5.5**). This shows that the Al doping and vacuum annealing increases the charge carrier concentration, ultimately affecting the work function[290].

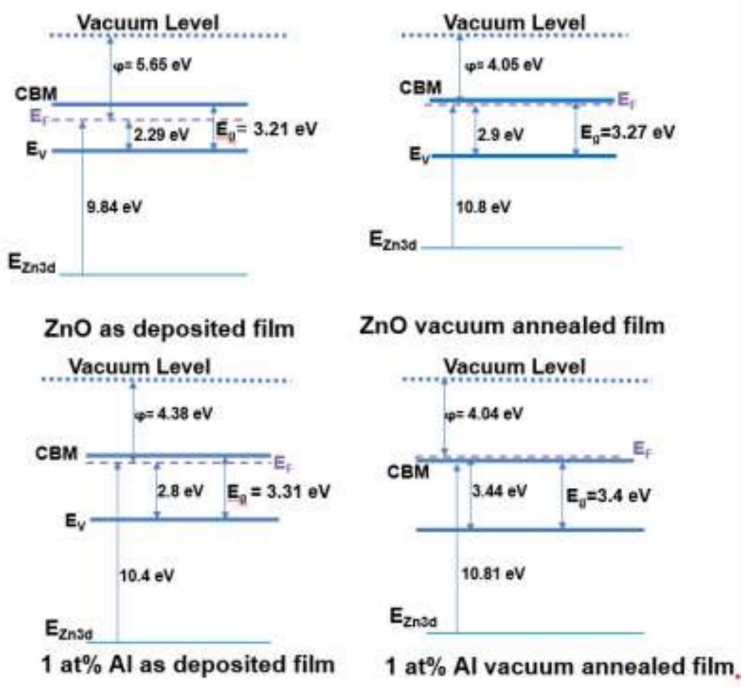

Figure 5.15 Energy level band diagram of zinc oxide thin film a) pure ZnO as-deposited b) vacuum annealed doped ZnO as-deposited c) 1AZO thin film as deposited d) 1AZO thin film vacuum annealed

5.3 Electrical properties of the film

Hall measurement, utilizing the Van der Pauw method, was carried out to characterize the electrical properties of films, and the results obtained are listed in

Table 5.4. An average of five measurements was taken. It was observed that in the case of pure ZnO, the resistivity was of the order of $3.82x10^{1}$ Ω-cm in the as-deposited sample, which decreased to $6x10^{-2}$Ω-cm on vacuum annealing, while in the case of as-deposited 1AZO, the resistivity was ~2.4 Ω-cm, which reduced to ~$2x10^{-3}$ Ω-cm on vacuum annealing. Charge mobility of electrons, sheet resistance, and charge carrier concentration for ZnO and 1AZO films were mentioned in **Table 5.5.** The increase in the oxygen vacancy after vacuum annealing leads to an increase in charge carrier concentration resulting in shifting the Fermi level (E_f) towards the conduction band. 1AZO film on vacuum annealing shows minimum resistivity of the order of ~10^{-3} Ω-cm due to an increase in mobility to ~50 cm^2/Vs and carrier concentration ~1.7 x $10^{20}cm^{-3}$ which is much greater as compared to the vacuum annealed pure ZnO thin film. It has earlier been argued that the creation of oxygen vacancies leaves behind two electrons which were believed to be the reason for the increase in carrier concentration. However, it has been shown that the V_O leaves behind deeper-level defects that are not so mobile and, as a result, do not play a significant role in conductivity; instead, the creation of Zn_i forms shallow defects. The two transitions Zn_i (+1/0) and Zn_i (+2/+1) act as shallow donors to contribute to the charge carrier concentration. This has also been observed by the XPS data, as explained in subsection **5.2.5**. Therefore, the presence of V_O and Zn_i, which caused the shift in Fermi level towards the conduction band edge, at the same time, vacuum annealing resulted in oriented morphologies (along (002) as shown by XRD) which reduces the scatter within the films making the vacuum annealed 1AZO films having a resistivity of the order of ~10^{-3} Ωcm^{-1}.

Table 5.5 Electrical properties of Al-doped and undoped zinc oxide films, as-deposited and vacuum annealed

Sample	n (10^{19} cm^{-3})	μ (cm^2/Vs)	SR (Ω/cm^2)x 10^2	ρ (Ω-cm)
As deposited				
Undoped ZnO	0.0026	14	5100	$3.82x10^1$
1AZO	0.18	13	302	2.4
After vacuum annealing				
Undoped ZnO	0.49	23	8.2	$6x10^{-2}$
1AZO	6.26	66	0.3	$2x10^{-3}$

n = Charge concentration, μ = Mobility, SR= sheet resistance, ρ = Resistivity

For applications as transparent contacts, the films must have a low resistivity and a low absorption coefficient(α) in the visible region. A way to evaluate this compromise is by means of the figure of merit (F_{TC}) [66] is defined as

$$F_{TC} \equiv \frac{1}{\alpha\rho} \qquad 5.5$$

The F_{TC} of the vacuum-annealed films for pure ZnO and 1AZO were $4x10^{-3}$ and 1.44, respectively. The F_{TC} reported earlier for solution-processed films is listed in **Table 5.6**. The F_{TC} achieved in this study is much better than the earlier reported values by solution processing. While doing spray pyrolysis of thin films, precursor solution was sprayed on the bare glass substrate in the ambient atmosphere to ensure the removal of organics/hydrates quickly. The presence of excess oxygen in the sample can lead to alumina formation and reduce the effectiveness of Al doping. Several authors have reported that annealing in the temperature range of 300-450°C helps in regaining conductivity[291, 292]. Some of the reports preferred annealing in forming gas leading to the annihilation of oxygen acceptor states at the grain

boundaries due to the desorption of oxygen, which acts as trap states for electrons [66, 96, 293]. On the other hand, other authors have reported the annealing of the film in the vacuum to regain higher conductivity [66,93].

Table 5.6 Figure of merit (F_{TC}) and deposition temperature of pure and Al-doped zinc oxide films prepared by solution processing

Pure/doped ZnO films	**Deposition temperature (^{0}C)**	**Figure of merit Ω^{-1} (F_{TC})**
ZnO [66]	420	2.45×10^{-7}
ZnO (vacuum annealed) [66]	420	5.19×10^{-6}
AZO [66]	420	4.56×10^{-7}
AZO (vacuum annealed) [66]	420	1.63×10^{-5}
AZO [201]	450	5.3×10^{-4}
AZO [294]	500	2.8×10^{-2}
AZO[201]	400	0.2
AZO [32]	400	8×10^{-4}
ZnO[32]	400	2×10^{-6}
AZO[202]	475	0.082
ZnO (H_2 atmosphere) [96]	400	3.12×10^{-3}
AZO (H_2 atmosphere)[96]	400	1.25×10^{-2}
AZO(N_2 atmosphere)[241]	500	5.24×10^{-3}
AZO (Ar atmosphere) [66]	400	2×10^{-4}
ZnO (Ar atmosphere) [66]	400	8×10^{-6}
ZnO [205]	470	0.01
AZO (our work)	*500*	*1.44*

It can be concluded that the extra carrier generation due to the formation V_O and Zn_i shifted the Fermi level closer to the CBM, reduced the work function, and therefore, increased the conductivity. The results show that vacuum/low-pressure annealing can be a viable route for achieving good conductivity in ZnO-based TCOs through solution processing routes.

5.4 Concluding Remarks

Pure and 1AZO films were prepared by spray pyrolysis route in the ambient atmosphere at 500 °C on a glass substrate using air as a carrier gas. The 1AZO films were oriented in [002] direction in as-deposited conditions, while the pure ZnO films became oriented on vacuum annealing. A columnar morphology was observed in scanning electron microscopy for 1AZO films having epitaxial growth, which was also confirmed from the topographical images of the AFM. Photoluminescence and XPS of O1s orbital of doped and undoped ZnO films showed an increase in Vo and Zn_i concentration after vacuum annealing of as-deposited films. The Vo and Zn_i gave rise to the free electrons close to the conduction band minima resulting in three order increase in the carrier concentration. In turn, it shifted the Fermi level to the higher energies. The maximum shift in Fermi level was observed in the case of vacuum-annealed Al-doped ZnO films. The Fermi level was at 3.21 and 3.31 eV for the pure and Al-doped films, which on vacuum annealing, increased to 3.27 eV and 3.4 eV, respectively. On vacuum annealing, the resistivity of pure and 1AZO film were ~ $6x10^{-2}$ and ~ $2x10^{-3}$ Ω-cm respectively. The results show that vacuum annealing is a viable means to enhance the electrical properties of the solution-processed 1AZO films. The processed 1AZO TCO on the glass substrate had a transparency of ~82% at 550 nm and resistivity of ~$2.11x10^{-3}$ Ω-cm with a figure of merit of 1.44.